ELSEVIER

Available online at www.sciencedirect.com
SCIENCE DIRECT®

Applied Surface Science 246 (2005) 290–302

applied surface science

www.elsevier.com/locate/apsusc

The effect of thermal contact resistance on heat management in the electronic packaging

M. Grujicic*, C.L. Zhao, E.C. Dusel

Department of Mechanical Engineering, Program in Materials Science and Engineering, Clemson University, Clemson, SC 29634, USA

Received 9 August 2004; accepted 12 November 2004
Available online 29 December 2004

Abstract

A finite element analysis is carried out in order to investigate the role of thermal contact resistance on heat management within a simple central processing unit (CPU)/heat sink assembly. A special attention is paid in assessing the effect of surface roughness characteristics, mechanical and thermal properties of the contacting bodies, applied contact pressures and the use of thermal interface materials on the maximum temperature experienced by the CPU. Two classes of thermal interface materials: (a) phase-change materials and (b) acrylic- or silicone-based tapes are considered. The results clearly reveal that plastic deformation of micro-contacts (promoted by high contact pressures and lower micro-hardness levels) and the use of thermal interface materials which eliminate (high thermal resistance) micro-gaps can significantly lower the overall CPU/heat sink thermal contact resistance and facilitate heat management. It is also shown that the retention of asperity micro-contacts and good wetting of the mating surfaces by the thermal interface material are critical for achieving an effective removal of the heat generated by the CPU.
© 2004 Elsevier B.V. All rights reserved.

PACS: 65.40.−b

Keywords: Thermal contact resistance; Heat management

1. Introduction

As the size of electronic devices continues to decrease and their clock speed continues to increase, management of the generated heat is becoming an evermore-important issue. Ineffective dissipation of the thermal energy threatens to limit not only the performance but also the life cycle and the reliability of electronic devices. Consequently, electronic packaging has transitioned from having the primary roles of providing interconnection and mechanical protection to the enclosed semiconducting device to serving as a conduit for transferring the heat from such a device to the environment.

* Corresponding author. Tel.: +1 864 656 5639; fax: +1 864 656 4435.
E-mail address: mica.grujicic@ces.clemson.edu (M. Grujicic).

0169-4332/$ – see front matter © 2004 Elsevier B.V. All rights reserved.
doi:10.1016/j.apsusc.2004.11.030

Nomenclature

A	area (m^2)
c_1	Vickers micro-hardness coefficient (GPa)
c_2	Vickers micro-hardness coefficient
C_p	constant-pressure specific heat (J/kg K)
C_Λ	gas specific constant (N/m K)
d	characteristic geometrical distance (m)
F	external force (N)
h	heat transfer coefficient (W/m^2 K)
H_{mic}	micro-hardness (Pa)
k	thermal conductivity (W/m K)
Kn	Knudsen number
m	mean absolute surface slope
M	gas parameter (m)
M_g	molecular weights of the gas (g/mol)
M_s	molecular weights of the solid (g/mol)
n	outward surface normal
n_s	number of micro-contacts
P	pressure (Pa)
Pr	Prandtl number
q	heat flux (W/m^2)
Q	heat source (W/m^3)
R	thermal resistance (K/W)
t	time (s)
T	temperature (K)
T_{inf}	temperature of the surrounding (K)
Y	mean surface plane separation (m)
z	local surface height (m)

Greek letters

α	thermal accommodation coefficient
γ	specific heat ratio
Λ	molecular mean free path (m)
μ	M_g/M_s
ρ	density (kg/m^3)
σ	RMS surface roughness (m)
σ'	σ/σ_0, where $\sigma_0 = 1$ μm

Subscripts

0	reference quantity
1,2	surface 1, 2 quantity
a	apparent quantity
c	contact quantity
n	nominal quantity
g	gas, micro-gap quantity
s	small, summit quantity

Superscript

*	normalized quantity

The main objective of thermal management in electronic packaging is the efficient removal of heat from the semiconducting device to the ambient environment. In general, this heat removal involves the following four major stages: (a) heat transfer within the device package itself; (b) heat transfer from the package to a heat sink; (c) heat transfer through the heat sink; and (d) heat transfer from the heat sink to the ambient environment. While each of the four heat transfer stages affects the rate of heat removal from a semiconducting device, the heat transfer between the package and the heat sink is generally considered the rate limiting process. That is the contacting surfaces between the package and the heat sink are generally neither fully conforming nor smooth. Rather, the surfaces are somewhat non-conforming and rough making the real contact area between the package and the heat sink is substantially smaller than the corresponding nominal contact surface area. Consequently, the heat transfer across the package/heat sink interface takes place through surface-asperity micro-contacts and through air-filled micro-gaps (Fig. 1(a)), and is, hence, associated with a significant thermal resistance (the so-called *thermal contact resistance*) [1].

To reduce the thermal contact resistance between a semiconductor package and a heat sink, a variety of materials commonly referred as *thermal interface materials* have been developed [2]. These materials are used to reduce or completely eliminate the air gaps from the contact interfaces by conforming to the rough and uneven mating surfaces (Fig. 1(b)). Because the thermal interface materials generally possess a higher thermal conductivity than the interfacial gas (air) they replace, the interfacial thermal resistance is reduced giving rise to a lower temperature of the electronic component junction. The efficiency of the thermal interfacial materials in reducing the interfacial thermal resistance depends on a number of factors among which thermal conductivity of the material and its ability to wet the mating surfaces appear to be the most significant. There are several classes of thermal interface materials. For the present purpose, we consider only two limiting classes of thermal interface materials:

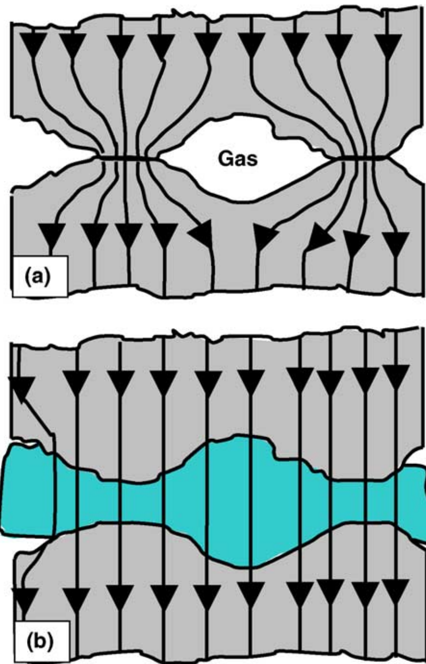

Fig. 1. A schematic of two contacting bodies: (a) in direct contact and (b) separated by a thermal interface material. The arrows denote the heat flow across the interface.

(a) Thermal greases and phase-change materials whose viscosity rapidly diminishes with an increase in temperature allowing them to freely flow throughout the thermal joint and fill the gaps which were initially present. This process typically requires the application of a small contact pressure to bring the two surfaces together and cause the thermal interface material to flow. While the thermal conductivity of these materials is relatively low (ca. 0.3 W/m K), they tend to wet the mating surfaces well while allowing retention of the (high thermal conductivity) asperity micro-contacts.
(b) On the other extreme are the materials such as conductive-particle filled acrylic- or silicone-based thermal tapes and pads. While these materials possess somewhat higher thermal conductivity (ca. 0.7 W/m K), they tend to eliminate (high thermal conductivity) asperity micro-contacts while not being able to fully fill the interfacial gaps.

Thus the two classes of thermal interface materials may display different levels of efficiency for reducing the thermal contact resistance, depending on the nature of the contacting materials, morphological and crystallographic characteristics of the mating surfaces and the process parameters for the thermal interface material application technique.

The objective of the present work is to carry out a finite element analysis of the heat transfer process within an electronic device attached to a heat sink in order to elucidate the role of thermal contact resistance on the efficiency of heat management. Specifically, efficiency of the two classes of thermal interface materials for reducing the maximum temperature of the electronic device is analyzed relative to the maximum temperature experienced by the same device when the interface between the device and the heat sink is not filled with a thermal interface material.

The organization of the paper is as follows. A brief description of the finite element problem analyzed in the present work including the governing differential equation, the boundary conditions and the solution method is discussed in Section 2.1. The phenomenon of heat transfer through conforming rough surfaces involving heat conduction through the asperity micro-contacts and through the interstitial-gas (air) filled micro-gaps are discussed in Section 2.2. The results obtained in the present work are presented and discussed in Section 3. The main conclusion resulted from the present work are summarized in Section 4.

2. Computational procedure

2.1. Problem definition

To quantify the effect of thermal contact resistance on the problem of heat management in electronic devices, a simple model for a central processing unit (CPU)/heat sink assembly is developed in the present model. For simplicity, the CPU is modeled as a (1 cm radius, 5 cm length) cylinder-shape semiconductor surrounded by an aluminum heat sink equipped with cooling fins, Fig. 2(a) and (b). A 25 μm wide contact region is assumed to exist between the CPU and the heat sink. The heat generated during the operation of the CPU is accounted for by treating the CPU as a volumetric heat source with a total power of 5 W. The outer-surface of the aluminum heat sink is assumed to be cooled by natural or forced convection.

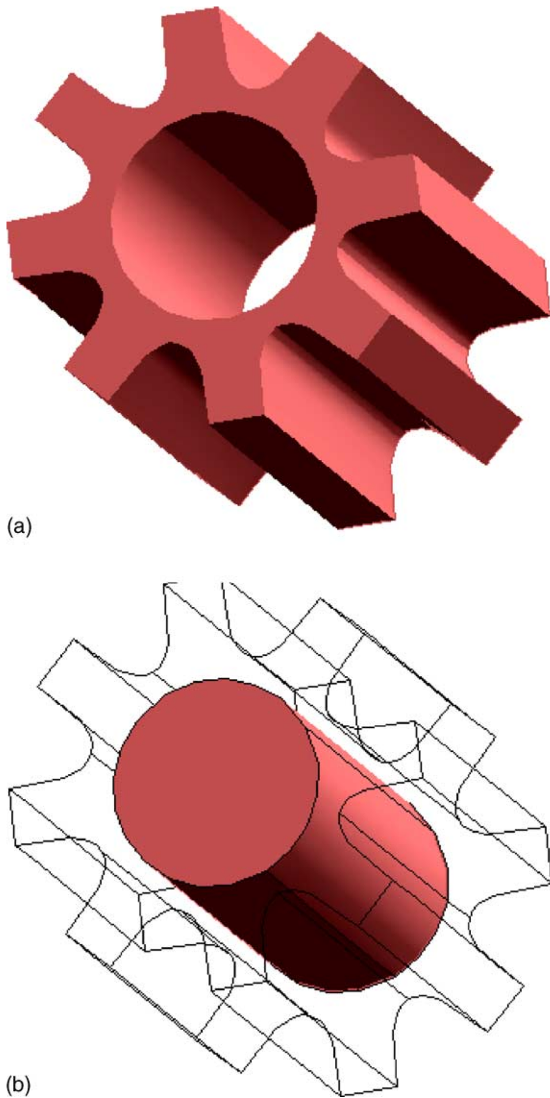

Fig. 2. A schematic of the geometries of (a) an aluminum heat sink and (b) a cylindrical silicon CPU core.

To further simplify the analysis, the heat transfer in the direction parallel with the CPU axis is not considered, and hence, the problem has been reduced to a two-dimensional formulation. The schematic shown in Fig. 3(a) suggests that due to the symmetry of the problem, only one-sixteenth of the CPU/heat sink cross section area needs to be modeled. A schematic of the resulting computational domain along with the governing differential equation and the boundary condition are given in Fig. 3(b).

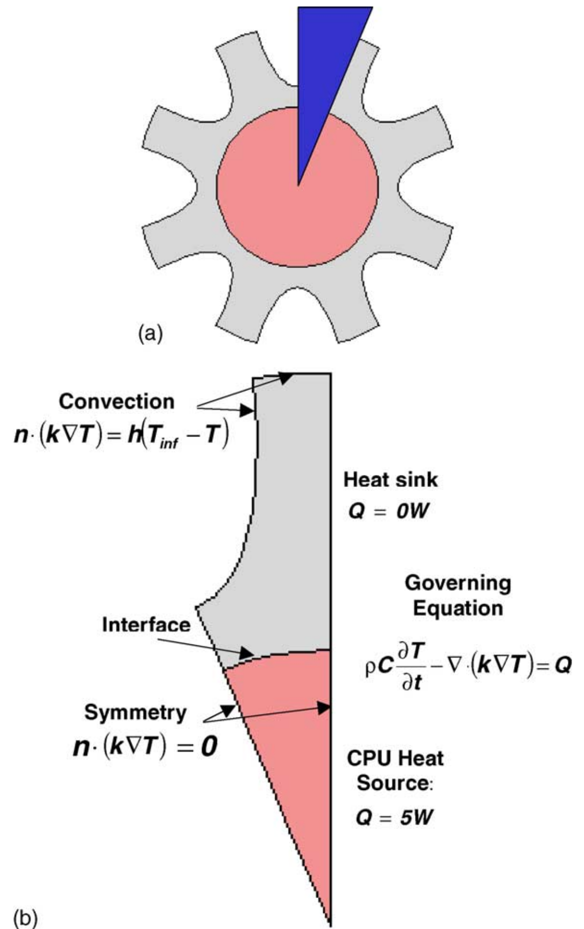

Fig. 3. (a) A two-dimensional model for the CPU/heat sink assembly. (b) One-sixteenth of the cross section used as the computational domain, the governing equations and the boundary conditions.

2.1.1. Governing differential equation

The temperature distribution within the CPU/heat sink assembly is governed by the following form of the energy conservation equation:

$$\rho C_p \frac{\partial T}{\partial t} - \nabla \cdot (k\nabla T) - Q = 0 \tag{1}$$

where ρ is the material density, C_p the constant-pressure specific heat, t the time, k the thermal conductivity and Q the volumetric heat source. The first term in Eq. (1) represents the energy accumulation term, the second term denotes the inlet/outlet heat-flux difference over a unit volume and the last term defines the volumetric heat source/sink term.

2.1.2. Boundary conditions

As shown in Fig. 3(b), all the boundary conditions in the present model are defined using the so-called *Neumann-type* conditions which specify the outward heat flux, $n\cdot(k\nabla(T))$, where n is the outward surface normal. At the outer-surfaces of the heat sink, the outer heat flux is set equal to the convective heat flux, $h(T_{\rm inf} - T)$, where h denotes the heat transfer coefficient and $T_{\rm inf}$ is the temperature of the surrounding. At the symmetry boundaries of the computational domain, the outward heat flux is set to zero. No heat transfer by radiation or the presence of surface heat sources/sink is considered.

The forced-convection heat transfer coefficient for the case of a cooling fan blowing air in a direction parallel with the axis of the heat sink is evaluated using the following procedure:

(a) For a typical value of the air temperature (298–350 K), air pressure (1 atm), air free-stream velocity (8.5 m/s, corresponding to a standard 10 ft^3/min cooling fan and an estimated volume of the free space surrounding the heat sink), the air properties are obtained from standard tabulations as: air density, $\rho = 1$ kg/m^3; the Prandtl number, $Pr = 0.7$; the kinematics viscosity, $\nu = 2.07 \times 10^{-6}$ m^2/s; the air thermal conductivity, $k = 0.0299$ W/m K.
(b) Using the aforementioned data, the Reynolds number has been evaluated as: $Re_L = \rho L/\nu = 2 \times 10^4$, where $L = 5 \times 10^{-2}$ m is the length of the heat sink;
(c) Next, it is assumed that roughness conditions of the outer surface of the heat sink can be selected in such a way that the turbulent flow is promoted at a critical value of the Reynolds number, $Re_{c,x} = 1 \times 10^4$.
(d) Then, the corresponding Nusselt number, Nu_L, is calculated as: $\mathrm{Nu}_L = (0.037(\mathrm{Re}^{4/5} - \mathrm{Re}_{x,c}^{4/5}) + 0.664\mathrm{Re}_{x,c}^{1/2}) = 100.13z$
(e) At last, the corresponding mean heat transfer coefficient, h, is evaluated as $h = Nu_L k/L$=59.9 W/m^2 K.

This value of the heat transfer coefficient is assigned to the outer surface of the heat sink.

Since the objective of the present analysis is to establish how the magnitude of the thermal contact resistance affects the maximum temperature of the CPU (i.e., the temperature at the center of the CPU), only a stationary (time-invariant) analysis is conducted in the present work. Consequently, the first (time-dependent) term in the governing equation, Eq. (1), is eliminated.

2.1.3. Computational method

The governing differential equation, Eq. (1), subjected to the boundary conditions specified in Fig. 3(b), is solved using the commercial mathematical package FEMLAB [3] and solved for the single dependent variable (temperature) using the finite element method (Fig. 4). FEMLAB provides a powerful interactive environment for modeling various scientific and engineering problems and for obtaining the solution for the associated (stationary and transient, both linear and nonlinear) systems of governing partial differential equations. FEMLAB is fully integrated with the MATLAB, a commercial mathematical and visualization package [4]. As a result, the models developed in the FEMLAB can be saved as MATLAB programs for parametric studies or iterative design optimization.

Standard mesh sensitivity and model robustness analyses are carried out following the procedure outlined in our recent work [5]. The results of these analyses validated that the model developed is mesh-insensitive and robust but the results are not be presented here for brevity.

2.2. Thermal contact resistance

As mentioned in the previous section, the contacting surfaces of the electronic device and the heat sink are mutually conforming but each of them is generally rough making the real contact surface area between the two bodies significantly smaller than the nominal surface area. In general, the surfaces of the two bodies may somewhat deviate from the ideal circular shapes in which case the contacting surfaces may not be fully conforming. The effect of such non-conformity of the contacting surfaces is not considered in the present paper. In other words, thermal resistance of the contacting surfaces is assumed to be governed only by their effective roughness, the presence of interstitial gases and/or thermal interface materials and the magnitude of the compressive contact pressures. The

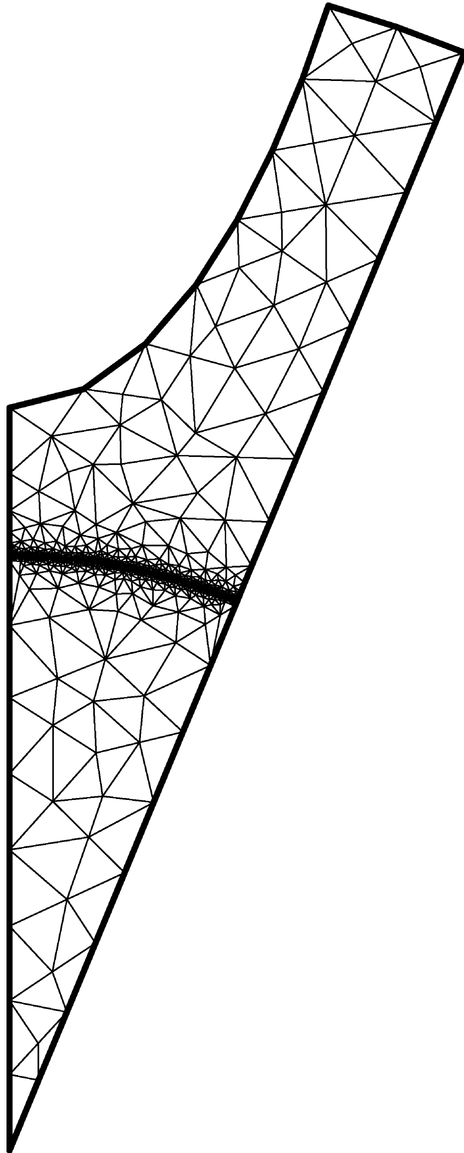

Fig. 4. A typical finite element mesh used in the present work consisting of 839 nodes and 1624 triangular elements.

resulting thermal contact resistance is analyzed using the semi-empirical model recently proposed by Bahrami et al. [6]. A brief overview of this model is given in this section.

When rough conforming surfaces are placed in mechanical contact, real contact occurs only at the top of touching surface asperities. If the roughness of the two surfaces is random, the resulting micro-contacts are also expected to be distributed randomly. The micro-contacts are generally located far from each other making the real contact area (a summation of all micro-contact areas) only a small portion (typically a few percent) of the nominal contact area. In mechanically fastened structures, the gaps between the micro-contacts are filled with an interstitial gas (typically air). In such cases, conduction through micro-contacts and the interstitial gas are the two main modes for the transfer of heat between the two contacting bodies. Thermal radiation across the interfacial gaps is generally considered as insignificant as long as the surface temperatures are less than approximately 700 K. Natural convection is also generally neglected as a heat transfer mode within the interfacial gaps due to the fact that the small thickness of interfacial gaps (typically less than 10 μm) makes the Grashof number (the ratio of buoyant to viscous forces) below 2000 [7]. Thus, conduction remains the main mode of heat transfer through the contact interfaces. Since the real contact surface area is relatively small and so is thermal conductivity of the interfacial gases, heat flow across the interface experiences a relatively large thermal resistance, commonly referred to as *thermal contact resistance*.

When the interfacial region between two bodies is filled with the so-called *thermal interface materials*, two typical scenarios may emerge: (a) the interfacial thermal material fills the interfacial gaps while allowing formation of the asperity micro-contacts. In this case, the interfacial heat transfer is controlled by conduction through the micro-contacts and through the thermal interface material; (b) the thermal interface material completely separates the two contacting bodies preventing formation of the micro-contacts. In this case, the interfacial heat transfer is controlled by thermal conduction through the thermal interface material alone. Both of these scenarios are considered in the present work. In the following sections, separate overviews are given of the thermal conduction through micro-contacts, interstitial-gas filled gaps, and the thermal interface material.

2.2.1. Micro-contact heat transfer

Experimental investigations of Williamson et al. [8] clearly established that many of the manufactur-

ing processes produce surfaces with an isotopic Gaussian distribution of heights of the surface asperities. In most analyses of the micro-contact resistance involving two rough Gaussian surfaces, the analysis can be simplified by considering the contact between a single surface (with effective or combined surface roughness characteristics) and a perfectly smooth surface, under the condition that the separation between the mean planes of the two surfaces remains uncharged. The equivalent root-mean-squared (RMS) roughness, σ, and the equivalent mean absolute surface slope, m, are respectively defined as

$$\sigma = \sqrt{\sigma_1^2 + \sigma_2^2} \quad \text{and} \quad m = \sqrt{m_1^2 + m_2^2} \tag{2}$$

where subscripts 1 and 2 are used to denote the two contacting bodies.

Thermal resistance associated with micro-contacts (also known as *thermal constriction/spreading resistance*) is generally modeled by applying the so-called *flux tube* solution to each micro-contact [9]. When the separation between micro-contacts is sufficiently large, as is generally the case, thermal constriction/spreading resistance can be modeled using the isothermal source on a half-space solution [10]. Bahrami et al. [11,12], combined the heat source on a half-space solution with a scaling analysis (primarily involving the observation that the mean radius of micro-contacts is proportional to the surface roughness, σ, and inversely proportional to the surface slope, m) and with the assumption that the asperities undergo plastic deformation, to propose the following relation for a single micro-contact resistance:

$$R_{s,i} = \frac{0.565 c_1 (\sigma/m)}{k_s F} \left(\frac{\sigma'}{m}\right)^{c_2} \tag{3}$$

where $\sigma = \sigma/\sigma_0$, $\sigma_0 = 1\ \mu\text{m}$, $k_s = 2k_1k_2/(k_1 + k_2)$ is the harmonic mean of solid thermal conductivities of the two bodies, F the applied load and c_1 and c_2 are Vickers-hardness correlation coefficients. A subscript i is used in Eq. (3) to denote that the expression defined by this equation pertains to thermal resistance of a single individual micro-contact.

Eq. (3) is used in the present work to assess the magnitude of thermal constriction/spreading resistance of a single micro-contact. Since the micro-contacts are connected in parallel in a single interface, the overall micro-contact resistance can be defined as

$$R_s = \left(\sum_{i=1}^{n_s} \frac{1}{R_{s,i}}\right)^{-1} \tag{4}$$

where n_s is the total number of micro-contacts which following Cooper et al. [13] can be defined as

$$n_s = \frac{1}{16}\left(\frac{m}{\sigma}\right)^2 \frac{\exp(-Y^2/\sigma^2)}{\operatorname{erf}(Y/\sqrt{2}\sigma)} A_a \tag{5}$$

where Y is mean-planes separation of the contacting surfaces (defined later).

2.2.2. Micro-gap heat transfer

The resistance to the heat transfer within the interfacial gaps filled with interstitial gas is considered in this section. Following Bahrami et al. [6], the heat transfer problem through the interfacial gaps is simplified to the heat transfer problem between two isothermal parallel plates (correspond to the surfaces of the two contacting bodies) which are located at an average (effective) distance, d, between each other.

In general, thermal conduction in a gas layer between two parallel plates is categorized into four heat-flow regimes: (a) continuum, (b) temperature jump or slip, (c) transition and (d) free molecule. The parameter which delineates these regimes is the Knudsen number which is defined as

$$Kn = \frac{\Lambda}{d} \tag{6}$$

where Λ and d are the molecular mean free path and the characteristic geometrical distance (the distance between the two plates in the present case).

The molecular mean-free path represents the average distance a gas molecule travels before it collides with another gas molecule and is proportional to the gas temperature and inversely proportional to the gas pressure as

$$\Lambda = C_\Lambda \frac{T_g}{P_g} \tag{7}$$

where T_g and P_g are respectively the gas temperature and pressure while C_Λ is a gas-specific constant.

In *the continuum gas-conduction regime*, where $Kn < 0.01$, the heat transfer between the plates takes place mainly via the collisions and energy exchange between the gas molecules. In this case, the rate of

heat transfer is independent of the gas pressure but varies with the gas temperature. As the gas pressure is reduced, the intermolecular collisions become less frequent and the energy exchange between gas molecules and the plates begins to affect the heat transfer between the plates. When $0.01 \leq Kn \leq 0.1$, the energy exchange at the plate/gas interfaces becomes incomplete resulting in a discontinuity of temperature at these interfaces (*the temperature-jump regime*). When the gas pressure start to approach vacuum conditions, $Kn \geq 10$, intermolecular collision are rare and the main mechanism for heat transfer between the plates is the energy exchange between the gas molecules and the plates. This regime of heat transfer is commonly referred to as *the free molecular* regime. In the intermediate regime, *the transition regime*, in which $0.1 \leq Kn \leq 10$, both the intermolecular collisions and the molecule/plate collisions make important contributions to the heat transfer between the plates.

Utilizing the Maxwell's theory for interfacial temperature discontinuity, Yovanovich et al. [14], proposed the following expression for the heat flux through a gas layer between two parallel plates for all four gas-phase regimes:

$$q_{\mathrm{g}} = \frac{k_{\mathrm{g}}}{d+M}(T_1 - T_2) \tag{8}$$

where q_{g} is the heat flux, T_1 and T_2, respectively the uniform temperatures of the two parallel plates, k_{g} the gas thermal conductivity and M the gas parameter (defined later).

Since thermal resistance can be generally defined as a ratio of the temperature difference and the corresponding heat rate, the micro-gap thermal resistance becomes

$$R_{\mathrm{g}} = \frac{d+M}{k_{\mathrm{g}}A_{\mathrm{g}}} \tag{9}$$

where A_{g} is the gap heat transfer area.

Following Song [15] and Yovanovich et al. [14], the gas parameter M is defined as

$$M = \left(\frac{2-\alpha_1}{\alpha_1} + \frac{2-\alpha_2}{\alpha_2}\right)\left(\frac{2\gamma}{1+\gamma}\right)\frac{1}{Pr}\Lambda \tag{10}$$

where α_1 and α_2 are thermal accommodation coefficients corresponding to the two gas/plate interfaces, γ the specific heats ratio for the interstitial gas and Pr the gas Prandtl number.

Thermal accommodation coefficient, α, quantifies the average fraction of the kinetic energy of a gas molecule which is exchanged during collision with the solid wall (plate surface). Thermal accommodation coefficient depends on the morphological and crystallographic conditions of the surface and on the gas/solid combination and following Song [15] and Yovanovich et al. [14] can be assessed using the following expression:

$$\alpha = \exp\left[-0.57\left(\frac{T_{\mathrm{s}} - T_0}{T_0}\right)\right]\left(\frac{M_{\mathrm{g}}^*}{6.8 + M_{\mathrm{g}}^*}\right) + \frac{2.4\mu}{(1+\mu)^2}\left\{1 - \exp\left[-0.57\left(\frac{T_{\mathrm{s}} - T_0}{T_0}\right)\right]\right\} \tag{11}$$

where

$$M_{\mathrm{g}}^* = \begin{cases} M_{\mathrm{g}} & \text{for monatomic gases} \\ 1.4M_{\mathrm{g}} & \text{for diatomic/polyatomic gases} \end{cases}$$

and $\mu = M_{\mathrm{g}}/M_{\mathrm{s}}$, and M_{g} and M_{s} molecular weights of the gas and the solid, and $T_0 = 273$ K is the reference temperature.

According to Eq. (9), the mean effective distance between the contacting bodies, d, must be known before the micro-gap thermal resistance can be assessed. In the case of contact of the Gaussian rough surfaces with the mean separation, Y, the average gap height, d, can be defined as

$$d = \int_{-\infty}^{Y} (Y - z)\Phi(z)\,\mathrm{d}z \tag{12}$$

where z is the local surface height with respect to the mean plane, and the Gaussian probability density is given as

$$\Phi(z) = \frac{1}{2\pi\sqrt{\sigma}}\exp\left(-\frac{z^2}{2\sigma^2}\right) \tag{13}$$

It is clear that the mean value of z is zero and its RMS value is equal to its standard deviation, σ.

Substitution of Eq. (13) into Eq. (12), and the use of the assumption $A_{\mathrm{g}} \approx A_{\mathrm{n}}$ where A_{n} is the nominal contact surface area, yields:

$$d = Y \tag{14}$$

Eq. (14) implies that the mean gap height is equal to the mean planes separation of the two surfaces.

Substitution of Eq. (14) into Eq. (9) and the use of the condition $A_g = A_n$ yields:

$$R_g = \frac{M+Y}{k_g A_a} \tag{15}$$

For confirming rough surfaces at which the asperities undergo plastic deformation, Cooper et al. [13] showed that the mean-planes separation, Y, is the following function of the applied pressure, $P = F/A_n$, and material micro-hardness, H_{mic}:

$$Y = \sqrt{2}\sigma\,\mathrm{erfc}^{-1}\left(\frac{2P}{H_{mic}}\right) \tag{16}$$

Eq. (9) in conjunction with the Eq. (16) is used in the present work to assess the micro-gap thermal resistance.

2.2.3. Thermal resistance of the thermal interface materials

As discussed in Section 1, two limiting classes of thermal interface materials are considered in the present work: (a) phase-change materials whose viscosity rapidly diminishes with an increase in temperature allowing them to freely flow throughout the thermal joint and fill the interfacial gaps while enabling retention of the (high thermal conductivity) asperity micro-contacts. Thermaflow™ T766 phase-change thermal interface material [16] with a typical thermal conductivity of 0.3 W/m K is used in the present work; and (b) acrylic- or silicone-based thermal tapes and pads, which are completely sandwiched between the two contacting bodies and, hence, tend to eliminate (high thermal conductivity) asperity micro-contacts. Thermattach® T414 thermally conductive adhesive tapes filled with Kapton™ with a typical thermal conductivity of 0.7 W/m K is used in the present work.

2.2.4. Overall thermal contact resistance

When the interfacial gaps are filled with an interstitial gas or with a thermal interface material while the surface asperity micro-contacts are allowed to form, the heat transfer between the two bodies can take place through either the micro-contacts or through the (filled or unfilled) micro-gaps, or through both. Under such circumstances, the overall thermal contact resistance, R_c, can be considered to involve two sets of thermal resistances in parallel, and can be defined as

$$R_c = \left(\frac{1}{R_s} + \frac{1}{R_g}\right)^{-1} \tag{17}$$

When the thermal interface materials used completely prevent the contact of the two bodies, the thermal contact resistance is dominated by that of the thermal interface material.

3. Results and discussion

3.1. Thermal micro-contact resistance

The model briefly reviewed in Section 2.2.1 is used in the present section to compute a typical value of the thermal micro-contact resistance for the silicon CPU/aluminum heat sink contacting surface. The reference values of the materials and surface parameters used in this section are listed in Table 1. While compiling these values it is considered that the contacting surfaces of both the silicon CPU and the aluminum heat sink are produced by cutting/machining and that the aluminum heat sink is most frequently produced by die casting. Aluminum is considered as the softer of the two materials and, hence, only its hardness properties are considered when assessing the thermal micro-contact resistance. A typical value of the

Table 1
Parameters used to compute the micro-contact thermal resistance

Parameter	Value	Equation where first used
RMS surface roughness, σ (m)	2×10^{-6}	Eq. (2)
Mean absolute surface slope, m	0.12	Eq. (2)
Thermal conductivity of silicon, k_1 (W/m K)	63	Eq. (3)
Thermal conductivity of aluminium, k_2 (W/m K)	232	Eq. (3)
External pressure, F (kPa)	25	Eq. (3)
Vickers micro-hardness coefficient for aluminium, c_1 (GPa)	6.23	Eq. (3)
Vickers micro-hardness coefficient for aluminium, c_2	−0.23	Eq. (3)

contact pressure 25 kPa is also used. The application of Eq. (4) in conjunction with Eq. (5) and with the material/surface parameters listed in Table 1, yielded the thermal micro-contact resistance of $R_s = 1.81 \times 10^{-3}$ K/W.

To assess the sensitivity of the thermal micro-contact resistance to the variations in the four key model parameters (the contact pressure, P, the aluminum micro-hardness, H_{mic}, the RMS roughness, σ, and the mean absolute roughness slope, m), the contact pressure in a range between 15 and 35 kPa, the aluminum micro-hardness in a range between 0.2 and 0.3 MPa, the surface roughness in a range between 1.0 and 3.0 μm and the asperity slope in a range between 0.06 and 0.18 are considered. The results of this calculation are shown as contour plots in Fig. 5(a) and (b). The RMS roughness, σ, and the mean absolute roughness slope, m, are set to their reference values in Fig. 5(a), while the contact pressure, P, and the aluminum micro-hardness, H_{mic}, are kept at their reference values in Fig. 5(b). It is seen that, as-expected, a higher contact pressure and a lower hardness, which promote plastic deformation of the asperities and the formation of micro-contacts with a larger contact surface area give rise to a lower value of the thermal micro-contact resistance. Likewise, an increase in the RMS roughness and a decrease in the roughness slope, which result in higher values of the micro-contact surface area, also give rise to the lower thermal micro-contact resistance values.

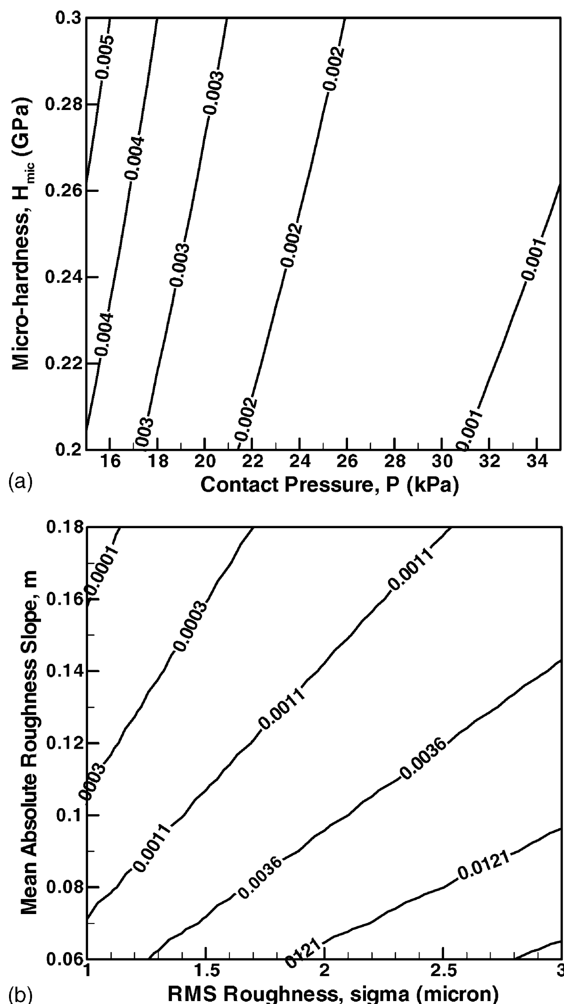

Fig. 5. The effect of contact pressure, micro-hardness, surface roughness and roughness slope on thermal micro-contact resistance.

The reference value of the thermal micro-contact resistance, $R_s = 1.08 \times 10^{-3}$ K/W, is used in the Section 3.3 to assess the effectiveness of thermal interface materials in reducing the thermal contact resistance between the CPU and the heat sink.

3.2. Thermal micro-gap resistance

The procedure described in Section 2.2.2 is used in the present section to compute the thermal interface resistance due to micro-gaps filled with nitrogen (used in place of air) at the atmospheric pressure. The parameters used to compute the thermal micro-gap resistance are given in Tables 1 and 2. Using Eq. (7), a reference contact pressure of 25 kPa and assuming that nitrogen is in a temperature range between the room temperature and 373 K, the Knudsen number has been computed as $Kn = 0.008$. Thus, the gas residing within the interfacial micro-gaps is in the continuum regime under these conditions. In fact, under all the conditions examined in the present work, nitrogen is found to be either in the continuum or in the temperature-jump regime.

For the reference values of the mechanical and surface parameters discussed in the previous section, the thermal micro-gap resistance is computed as $R_g = 8.78 \times 10^{-2}$ K/W. This value is used in the next section to assess the effectiveness of thermal interface materials in reducing the thermal contact resistance.

The effect of the four key material/surface parameters (P, H_{mic}, σ and m) on the thermal micro-gap resistance is displayed as contour plots in

Table 2
Parameters used to compute the gap thermal resistance

Parameter	Value	Equation where first used
Thermal accommodation coefficient, α	0.78	Eq. (10)
Specific heat ratio, γ	1.4	Eq. (10)
Prandtl number, Pr	0.69	Eq. (10)
Mean free path constant, C_A (m)	62.8×10^{-9}	Eq. (6)
Gas pressure, P_g (Torr)	50	Eq. (7)
Thermal conductivity of gas, k_g (W/m K)	0.031	Eq. (8)

Fig. 6(a) and (b). As expected, a higher P, a lower H_{mic}, and a lower σ, which all lead to a lower thickness of the interfacial micro-gaps, give rise to a lower values of the thermal micro-gap resistance. The mean absolute roughness slope, m, on the other hand does not affect the thermal micro-gap resistance, at least within the scope of the present model.

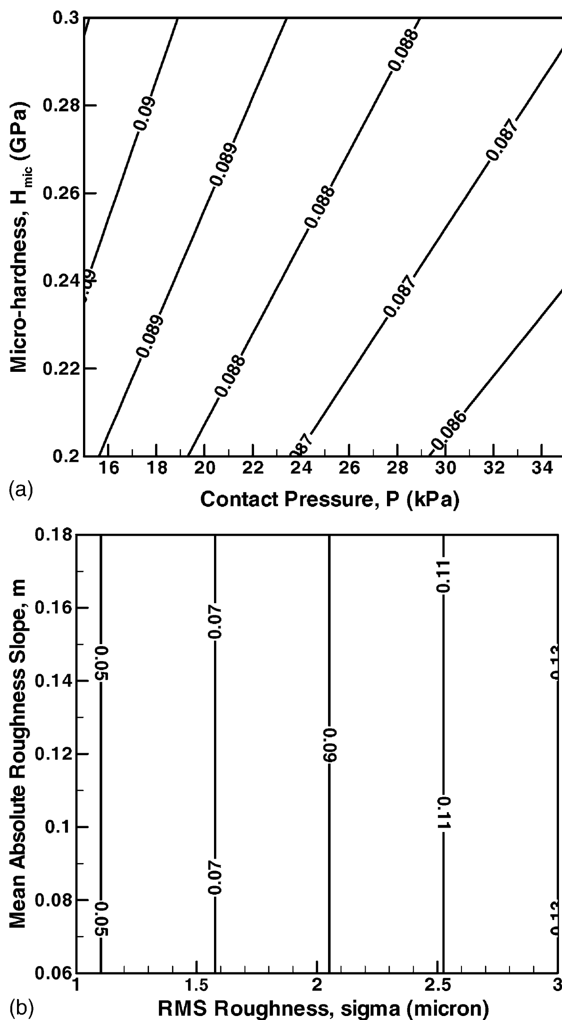

Fig. 6. The effect of contact pressure, micro-hardness, surface roughness and roughness slope on thermal micro-gap resistance.

3.3. Heat management of the CPU/heat sink assembly

The values for the thermal micro-contact resistance, $R_s = 1.81 \times 10^{-3}$ K/W, and for the thermal micro-gap resistance, $R_g = 8.78 \times 10^{-2}$ K/W, are used in Eq. (17) to compute the overall thermal contact resistance under the condition when the micro-gaps contain interstitial gas (nitrogen). The resulting value, $R_c = 1.78 \times 10^{-3}$ K/W, is next used to compute the effective thermal conductivity of the 25 μm thick CPU/heat sink interface as $k_c = d/A_nR_c = 0.357$ W/m K. This value of the thermal conductivity is next assigned to the 25 μm thick CPU/heat sink interfacial region in Fig. 4 and the finite element analysis described in Section 2.1 carried out to determine the temperature distribution throughout the computational domain. The results of this calculation are shown in Fig. 7(a). It is seen that, as-expected, there is a sharp temperature drop across the CPU/heat sink interface. The maximum temperature of the CPU, i.e., the temperature at the center of the CPU, is found to be 336.7 K.

To assess the efficiency of thermal interface materials in reducing the thermal contact resistance and, thus, in reducing the maximum temperature experienced by the CPU, the interstitial nitrogen is replaced with these materials. As discussed earlier two classes of thermal interface materials are considered in the present work: (a) phase-change materials and (b) acrylic- or silicone-based tapes/pads. These two types of thermal interface materials are treated separately in the following.

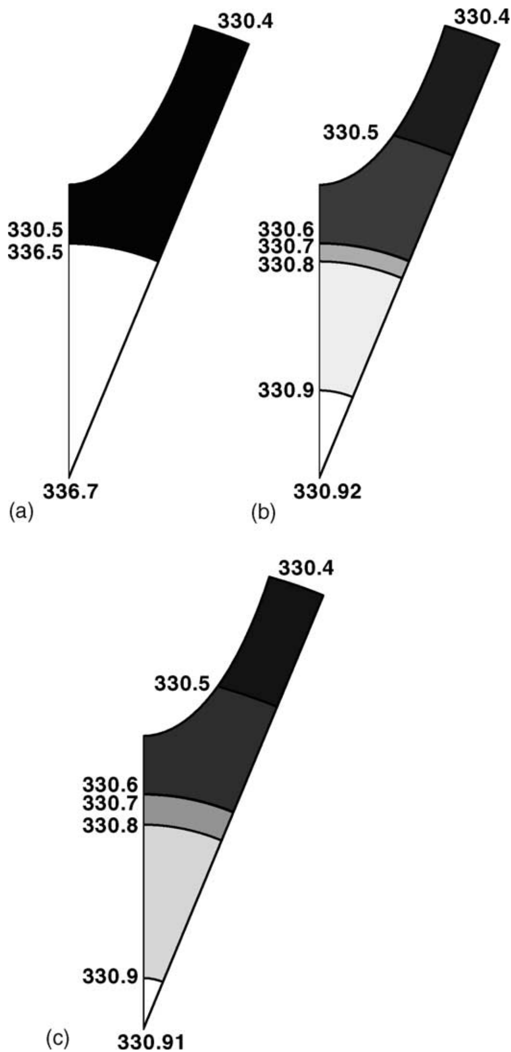

Fig. 7. The effect of thermal contact resistance and of the use of thermal interface materials on temperature distribution (in K) in a CPU/heat sink assembly. Please see the text for details.

First, the value for thermal micro-gap resistance, $R_g = 8.78 \times 10^{-2}$ K/W is replaced with a 25 μm-thick layer of Thermaflow™ T766 phase-change thermal interface material with a typical value of the thermal conductivity of 0.3 W/m K [16] and Eq. (17) used again to compute the overall thermal contact resistance, R_c. The resulting value for R_c is next used to determine the corresponding thermal contact conductivity, $k_c = d/A_nR_c = 0.56$ W/m K. The latter is then assigned to the 25 μm-thick CPU/heat sink interface and the finite element analysis carried out again. The results of this analysis are shown in Fig. 7(b). The results displayed in Fig. 7(b) show that the use of Thermaflow™ T766 phase-change thermal interface material reduces the temperature drop across the CPU/heat sink interface while lowering the maximum temperature of the CPU to 330.92 K (a near 6 K temperature decrease relative to the case shown in Fig. 7(a)).

Next, for the case of the Thermattach® T414 thermally conductive adhesive tapes filled with Kapton™, the thermal contact conductance (k_c) is assigned a typical value 0.7 W/m K for the thermal conductivity of this thermal interface material. As explained earlier, in the case of the Thermattach® T414, the two contacting bodies are completely separated from each other by the thermal interface material. Consequently, micro-contacts are not formed and Eq. (17) should not be used. The results of the finite element analysis for the case of Thermattach® T414 thermal interface material are shown in Fig. 7(c). The maximum temperature of the CPU in this case is 330.91 K, which is slightly lower than the corresponding value in the case of Thermaflow™ T766 phase-change thermal interface material.

The results presented in Fig. 7(a)–(c), clearly show that the use of thermal interface materials, which lower the thermal contact resistance can reduce the maximum temperature of the CPU by several degrees. This effect would be even more pronounced if a larger CPU which generates more power were analyzed. The other important observation which can be made by comparing the results displaced in Fig. 7(b) and (c) is that the phase-change materials, despite their lower thermal conductivity, are equally effective in reducing the maximum temperature experienced by the CPU. This is a result of the fact that these materials enable the retention of high thermal conductivity micro-contacts. If fact, considering that the acrylic- or silicone-based thermal interface tapes, such as Thermattach® T414, do not usually completely wet the surfaces of the contacting bodies and, hence, leave some micro-gaps unfilled, acrylic- or silicone-based thermal interface materials are expected to be somewhat less effective in reducing the maximum temperature of the CPU than predicted by the present model. Thus, the phase-change thermal interface materials appear to be a more attractive alternative. This is particularly the case considering the fact that, as shown in our recent work [17], the conductivity of these materials can be substantially increased (by over an order of magnitude) by the addition of single-walled

carbon nanotubes, which attain the percolation threshed at a very low loading level (less than ca. 0.1 vol.%). At the same time, the wetting characteristics of these materials are not measurably compromised by the addition of single-walled carbon nanotubes.

4. Conclusions

Based on the results obtained in the present work, the following main conclusions can be drawn:

1. Surface roughness properties as well as mechanical and thermal material properties can have a significant effect on the magnitude of the electronic-device/heat-sink thermal contact resistance and, hence, on the associated heat management.
2. Thermal interface materials can also have a significant role in lowering thermal contact resistance by reducing or eliminating (high thermal resistance, interstitial as filled) micro-gaps. These materials can be especially effective if they fully wet the contacting surfaces while allowing retention of the (high thermal conductivity) micro-contacts.
3. The magnitude of the thermal contact resistance can have a major role in heat management of electronic devices and, hence, may significantly affect performance, reliability and life cycle of such devices.

Acknowledgements

The material presented in this paper is based on work sponsored by the US Air Force through Touchstone Research Laboratory Ltd. The authors acknowledge valuable assistance of discussions with Professor Jay Ochterbeck of Clemson University.

References

[1] M. Bahrami, J.R. Culham, M.M. Yovanovich, G.E. Schneider, Review of thermal joint resistance models for non-conforming rough surfaces in a vacuum, in: Proceedings of the ASME Heat Transfer Conference, Paper No. HT2003-47051, July 21–23, Rio Hotel, Las Vegas, NV, 2003.
[2] E.S. Beyne, C.J. Lasance, J. Berghmans, Thermal management of electronics systems – II, in: Proceedings of the Eurotherm Seminar 45, September 20–22, Leuven, Belgium, 1995, p. 0792346122.
[3] FEMLAB 3.0a, COMSOL Inc., Burlington, MA, 2004. http://www.comsol.com.
[4] The Language of Technical Computing, MATLAB, 6th ed. The MathWorks Inc., Natick, MA, 2003.
[5] M. Grujicic, K.M. Chittajallu, Design and optimization of polymer electrolyte membrane (PEM) fuel cells, Appl. Surf. Sci. 227 (2004) 56–72.
[6] M. Bahrami, J.R. Culham, M.M. Yovanovich, Thermal resistances of gaseous gap for conforming rough contacts, in: Proceedings of the 42nd AIAA Aerospace Meeting and Exhibit, AIAA Paper No. 2004-0821, January 5–8, Reno, NV, 2004.
[7] W.H. McAdams, Heat Transmission, McGraw-Hill, New York, 1954.
[8] J.B. Williamson, J. Pullen, R.T. Hunt, D. Leonard, The Shape of Solid Surfaces, Surface Mechanics, ASME, New York, 1969, pp. 24–35.
[9] M.G. Cooper, B.B. Mikic, M.M. Yovanovich, Thermal contact conductance, Int. J. Heat Mass Trans. 12 (1969) 279–300.
[10] H.S. Carslaw, J.C. Jaeger, Conduction of Heat in Solids, 2nd ed. Oxford University Press, London, UK, 1959.
[11] M. Bahrami, J.R. Culham, M.M. Yovanovich, G.E. Schneider, Thermal contact resistance of non-conforming rough surfaces. Part 1. Mechanical model, in: Proceedings of the 36th AIAA Thermophysics Conference, AIAA Paper No. 2003-4197, June 23–26, Orlando, FL, 2003.
[12] M. Bahrami, J.R. Culham, M.M. Yovanovich, G.E. Schneider, Thermal contact resistance of non-conforming rough surfaces. Part 2. Thermal model, in: Proceedings of the 36th AIAA Thermophysics Conference, AIAA Paper No. 2003-4198, June 23–26, Orlando, FL, 2003.
[13] M.G. Cooper, B.B. Mikic, M.M. Yovanovich, Thermal contact conductance, Int. J. Heat Mass Trans. 12 (1969) 279–300.
[14] M.M. Yovanovich, J.W. DeVaal, A.A. Hegazy, A statistical model to predict thermal gap conductance between conforming rough surfaces, in: Proceedings of the AIAA/ASME third Joint Thermophysics, Fluids, Plasma and Heat Transfer Conference, AIAA Paper No. 82-0888, June 7–11, St. Louis, Missouri, 1982.
[15] S. Song, Analytical and experimental study of heat transfer through gas layers of contact interfaces. Ph.D. Thesis, University of Waterloo, Department of Mechanical Engineering, Waterloo, Canada, 1988.
[16] in: http://www.chomerics.com/products/thermflowT766.htm.
[17] M. Grujicic, G. Cao, W.N. Roy, A computational analysis of the percolation threshold and the electrical conductivity of carbon nanotubes reinforced polymeric materials, J. Mater. Sci. 39 (2004) 1–12.